

# A spectrophotometric catalogue of HII galaxies <sup>★</sup>

Cristina C. Popescu<sup>1,2</sup> and Ulrich Hopp<sup>3</sup>

<sup>1</sup> Max Planck Institut für Kernphysik, Saupfercheckweg 1, D-69117 Heidelberg, Germany

<sup>2</sup> The Astronomical Institute of the Romanian Academy, Str. Cuțitul de Argint 5, 75212, Bucharest, Romania

<sup>3</sup> Universitätssternwarte München, Scheiner Str.1, D-81679 München, Germany

Received; accepted

**Abstract.** We present a spectrophotometric catalogue of 90 emission-line galaxies (ELGs) discovered during an objective - prism survey that aimed to search for dwarf galaxies within the voids (Popescu et al. 1996, 1998). The paper presents line ratios, equivalent widths and absolute fluxes for the emission-lines seen in the spectra of the galaxies. A list of newly discovered Wolf-Rayet galaxies is presented. Many objects included in the catalogue have low metallicity and the extreme cases are proposed as candidates for very low metallicity galaxies.

**Key words:** galaxies: compact - galaxies: dwarf - galaxies: abundances - galaxies: statistics - galaxies - distances and redshifts - large scale structure of Universe

## 1. Introduction

Popescu et al. (1996, 1998) conducted a survey for emission-line galaxies (ELGs) based on the Hamburg Quasar Survey (HQS, Hagen et al. 1995) - IIIa-J digitised objective prism plates. The main goal of the project was to search for dwarf ELGs in voids and to analyse the large-scale structure of the distribution of this kind of galaxies (Popescu et al. 1997). The follow-up spectroscopy at the 2.2m telescope at the German-Spanish Observatory at Calar Alto (Almeria, Spain) provided us with a complete sample of 250 ELGs, of which many are Blue Compact Dwarfs (BCDs) or HII galaxies. These two terms are usually used to define the same kind of objects. While the name BCD was mainly used for objects classified on morphological criteria (Binggeli et al. 1985 - for the Virgo Cluster Catalogue), the term of HII galaxy was introduced for objects discovered on spectroscopic surveys for emission-line galaxies. These objects have focused attention after the discovery by Sargent & Searle (1970) that some of them were low metallicity systems hosting a very active stellar formation. Gallagher & Hunter (1989)

*Send offprint requests to:* Cristina C. Popescu (email address: popescu@levi.mpi-hd.mpg.de)

<sup>★</sup> Based on observations obtained at the German-Spanish Observatory at Calar Alto, Almeria, Spain

showed that the BCDs present also the lowest mass surface density and rotation velocities ever measured for objects supporting star formation activity. Thus it was suggested (Vilchez 1995) that these galaxies can be easily affected by environmental factors. Since in our study of the spatial distribution of ELGs (Popescu et al. 1997) we identified the isolation of each sample galaxy, we can address the question of environmental influences on the star-forming properties of HII galaxies, using an unbiased sample. In this paper we give the catalogue of the spectroscopic parameters of a subsample of 90 ELGs and we describe the data sample. The influence of the environment on the mechanism that controls star formation is discussed in a separate paper (Popescu et al. 1999).

## 2. The data

From our sample of 250 ELGs we selected for analysis only objects from a region North of the “Slice of the Universe” (de Lapparent et al. 1986), which is dominated by very well defined nearby voids. This subsample consists of 90 ELGs, most of them being distributed in the sheets and filaments that surround the voids, and with a few ELGs within some nearby voids or at the rim of the voids. No rich cluster of galaxies was included in the survey.

Most of the galaxies from this sample were observed twice. The objects were first observed in a snap-shot mode (Popescu et al. 1997), in order to check the selection criteria and to measure redshifts. In these campaigns we mostly did not have photometric conditions, therefore no reliable absolute fluxes could have been derived. Also a slit width of 2'' was used, which did not provide a total coverage of the galaxies. The observing campaign from May 1997 (see Table 1 for the details of the observations) was dedicated to the spectrophotometry of our objects, but it also completed the observations of selected candidates. These latter observations were done in good photometric conditions, with a slit width of 4''. For the small projected sizes of our dwarf galaxies, such an aperture is large enough to encompass most of their line emission. For the purpose of estimating the fraction of the line emission included in the slit we list in all the relevant tables of the paper the

**Table 1.** The details of the spectroscopic observations from May 1996

Detector	Lor-80
Pixel Size ( $\mu$ )	15
Slit width ( $\mu$ )	4
P.A.	90.
Pixel number	1024×1024
Grism	9
Dispersion ( $\text{\AA}/\text{pixel}$ )	5.6
Resolution ( $\text{\AA}$ )	17
Spectral Range ( $\text{\AA}$ )	3600-9000

seeing-corrected angular sizes of the star-forming HII regions ( $r_{HII}$ ). The comparison between the angular sizes of the emitting regions and the aperture sizes lead to the conclusion that the fluxes measured in the campaign from May 1996 represent accurate measurements of the total integrated fluxes of our galaxies. The large aperture used to obtain total fluxes reduces the resolution of our spectra, therefore any deblending of the emission lines was performed on the spectra taken in the previous campaigns. For the few galaxies observed only in the May 1997 observing campaign, no deblending was performed on the lines. Also, for the galaxies observed only in non-photometric conditions, no fluxes were assigned, only relative line ratios.

**Table 2**

error	emission line flux or equivalent width
5%	$H\beta$ , [OIII] $\lambda 4959$ , [OIII] $\lambda 5007$ , $H\alpha$ , $W([OIII])$ , $W(H\alpha)$
10%	[OII] $\lambda 3727$ , $H\gamma$ , HeI $\lambda 5876$ , $W(H\beta)$
15%	$H\delta$ , [SII] $\lambda 6717, 6731$
20%	[OI] $\lambda 6300$ , HeI $\lambda 6678$ , HeII $\lambda 4686$ , $W([SII])$
25%	HeI $\lambda 7065$ , [AIII] $\lambda 7136$
30%	[OI] $\lambda 6364$

The data were reduced using the MIDAS routines (as described by Popescu et al. 1996, 1998). The photometric calibrations of the spectra taken in the May 97 observing run were done using the standard stars: HZ 21, HZ 44 and BD +33°2642 (Oke 1990) and the absolute fluxes are accurate to about 10%. For one observing night the accuracy of the photometry was as good as 5%. Fluxes and equivalent widths of the emission lines were measured inter-actively using the integrate/line routine in MIDAS. The errors in the measurements were derived from repeated

observations of the lines, and the errors of the fluxes and equivalent widths  $W$  for different lines are given in Table 2.

For all the galaxies with a strong underlying continuum emission (relative to the  $H\beta$  line emission,  $W(H\beta) < 20 \text{\AA}$ ) we corrected the  $H\beta$  fluxes for underlying stellar absorption with an assumed constant equivalent width of  $2 \text{\AA}$  (McCall et al. 1985). The  $H\beta$  fluxes were afterwards corrected for reddening due to dust in our own Galaxy and in the galaxy being observed. We used the reddening coefficient  $c(H\beta)$ , derived from the observed  $H\alpha/H\beta$  Balmer line ratios. From equation (7.6) of Osterbrock (1974), the intrinsic ratio  $I(H\alpha)/I(H\beta)$  is related to the observed ratio via

$$\frac{F(H\alpha)}{F(H\beta)} = \frac{I(H\alpha)}{I(H\beta)} \times 10^{-c(H\beta)[f(H\alpha)-f(H\beta)]} \quad (1)$$

For the extinction in our Galaxy,  $f(H\alpha) - f(H\beta)$  is the standard Galactic reddening law (Whitford 1958), with the extinction values taken from Burstein & Heiles (1984). For the external extinction  $f(H\alpha) - f(H\beta)$  is the reddening law given by Howarth (1983), which should be closer to the average reddening law for the dwarf galaxies in our sample than the standard galactic one. We assumed that the intrinsic Balmer-line ratios are equal to the case B recombination values of Brocklehurst (1971) for an electron temperature of  $10^4 \text{ K}$  and an electron density of  $100 \text{ cm}^{-3}$ .

For all the objects considered in this paper we also obtained B and R frames. Most of the direct images were either obtained for the purpose of acquisition of the following spectroscopy or as a snap-shot survey to obtain total magnitudes. Dedicated deeper (600 sec B and 300 sec R) images were observed for all isolated ELGs. The photometry of the whole sample is discussed in detailed in Ven- niki et al. (1999). Based on their photometric parameters (absolute magnitudes, diameters) and the morphological appearance on the CCD images, the galaxies were classified into the morphological classes proposed by Salzer et al. (1989a,b), namely Star Burst Nucleus Galaxies (SBN), Dwarf Amorphous Nuclear Starburst Galaxies (DANS), HII Hotspot Galaxies (HIIH), Dwarf HII Hotspot Galaxies (DHIIH), Sargent-Searle Objects (SS), Magellanic Irregular (Im), and Interacting Pairs (IP). Nevertheless, an independent check was done using the line ratios of the emission-lines and their location in the diagnostic diagrams, and there is an overall good agreement between the morphological and spectroscopic classification.

Table 3

(1) Galaxy	(2) $M_B$	(3) z	(4) c(H $\beta$ )	(5) H $\beta$ W[ $\text{\AA}$ ]	(6) [OIII] W[ $\text{\AA}$ ]	(7) H $\alpha$ W[ $\text{\AA}$ ]	(8) [SII] W[ $\text{\AA}$ ]	(9) F(H $\beta$ ) <sub>obs</sub> [erg s <sup>-1</sup> cm <sup>-2</sup> ]	(10) r <sub>HII</sub> ["]	(11) type
HS1222+3741	-17.67	0.0409	0.151	114	681	593	39	1.67e-14	0.6	Im/BCD
HS1223+3938	-18.73	0.0360	0.474	15	91	101	14	6.88e-15	1.7	HIII
HS1232+3846	-19.70	0.0528	0.254	11	14	75	23	4.18e-15	2.0	SBN
HS1232+3947	-17.16	0.0210	0.286	29	139	172	13	8.90e-15	1.7	DHIII
HS1232+3612	-19.77	0.0425	0.411	18	85	136	25	1.27e-14		IP
HS1236+3821	-17.06	0.0073	0.602	4	23	37	9	7.72e-15	2.1	DHIII
HS1236+3937	-15.67	0.0184	0.081	112	506	521	56	5.72e-15	0.8	DHIII/SS
HS1240+3755	-21.1	0.0860	0.969	3	6	64	14	-		IP/SBNpec
HS1244+3648	-18.82	0.0472	0.000	35	146	140	38	1.52e-14	0.8	HIII
HS1256+3505	-18.75	0.0342	0.448	20	55	155	32	1.60e-14	1.1	DANS
HS1258+3438	-16.4	0.0248	0.380	36	209	189	15	4.39e-15		DHIII
HS1301+3312	-17.41	0.0371	0.391	31	125	177	40	5.90e-15	0.8	IP
HS1301+3325	-16.96	0.0246	0.573	11	51	73	8	3.71e-15	1.3	DHIII
HS1301+3209	-17.06	0.0238	0.579	10	36	78	13	3.01e-15	2.2	HIII
HS1304+3529	-17.38	0.0165	0.013	118	570	617	76	4.82e-14	1.9	IP
HS1306+3320	-18.32	0.0270	0.508	36	116	199	27	1.32e-14	1.9	HIII
HS1308+3044	-17.92	0.0209	0.564	4	13	40	8	4.55e-15	2.5	DANS
HS1311+3628	-16.84	0.0031	0.160	301	1550	1834	139	-		DHIII
HS1312+3847	-18.77	0.0515	0.037	74	337	392	58	1.53e-14	1.4	HIII
HS1312+3508	-16.26	0.0035	0.164	254	1466	1463	179	1.02e-13		DHIII
HS1315+3132	-16.46	0.0315	0.476	36	136	175	28	4.14e-15	0.8	DHIII
HS1318+3239	-17.22	0.0435	0.186	79	464	394	32	5.75e-15	1.2	IP
HS1319+3224	-15.3	0.0182	0.208	49	241	237	12	-	0.8	SS/DHIII
HS1325+3225	-17.9	0.0504	0.542	39	102	208	31	-		DHIII/HIII
HS1325+3255	-15.92	0.0263	0.146	74	412	340	14	4.38e-15	0.8	DHIII/SS
HS1327+3126	-18.07	0.0568	0.192	91	514	484	42	1.07e-14	0.6	DHIII
HS1328+3424	-17.79	0.0227	0.503	8	18	54	4	2.15e-15		HIII
HS1329+3703	-19.11	0.0557	0.214	7	9	54	15	-	1.9	HIII/DANS
HS1330+3651	-17.15	0.0167	0.147	72	387	371	45	2.62e-14		DHIII
HS1332+3426	-16.14	0.0220	0.444	35	167	195	17	4.27e-15	1.4	DHIII
HS1334+3957	-15.32	0.0083	0.000	71	351	334	26	-	1.8	DHIII
HS1336+3114	-17.94	0.0158	0.000	5	11	29	14	-	3.9	HIII
HS1340+3307	-16.63	0.0158	0.539	20	108	128	23	9.73e-15	1.6	DHIII
HS1341+3409	-16.35	0.0171	0.480	15	59	85	19	5.34e-15	1.2	DHIII
HS1347+3811	-15.30	0.0103	0.243	64	363	290	33	8.62e-15	4.9	DHIII
HS1349+3942	-15.16	0.0054	0.337	13	45	85	23	1.05e-14	1.8	DHIII
HS1354+3634	-17.10	0.0167	0.513	19	50	123	26	1.12e-14	1.2	DANS
HS1354+3635	-17.81	0.0171	0.507	21	76	124	25	2.04e-14	3.3	HIII
HS1402+3650	-18.81	0.0347	0.561	26	85	192	43	1.36e-14	1.6	HIII
HS1410+3627	-18.11	0.0338	0.311	15	55	97	28	5.16e-15		HIII
HS1413+4402	-19.67	0.0698	0.607	10	5	99	13	-	1.3	SBN
HS1416+3554	-16.94	0.0103	0.328	14	49	91	24	7.70e-15	3.4	HIII/DHIII
HS1420+3437	-16.75	0.0246	0.448	27	56	149	17	7.53e-15	0.6	DHIII
HS1422+3325	-17.30	0.0341	0.337	20	50	119	30	4.69e-15	0.8	HIII
HS1422+3339	-16.4	0.0114	0.350	17	58	95	20	1.12e-14	1.8	DHIII
HS1424+3836	-16.06	0.0218	0.195	104	579	545	24	1.00e-14	1.4	DHIII?
HS1425+3835	-17.80	0.0223	0.099	12	24	64	9	-	1.8	HIII
HS1429+4511	-17.40	0.0321	0.307	15	2	96	32	-	1.0	DANS
HS1429+3154	-16.73	0.0117	0.143	34	144	162	26	2.06e-14	2.6	DHIII
HS1438+3147	-17.88	0.0443	0.308	35	188	198	30	6.54e-15	1.2	DANS
HS1440+4302	-15.07	0.0085	0.336	44	269	238	31	1.13e-14	1.2	DHIII/SS
HS1440+3120	-17.4	0.0525	0.221	152	925	845	62	9.60e-15	0.7	DHIII
HS1440+3805	-18.80	0.0322	0.263	7	14	46	17	-	2.9	HIII

**Table 3 (continued)**

(1) Galaxy	(2) $M_B$	(3) z	(4) c(H $\beta$ )	(5) H $\beta$ W[ $\text{\AA}$ ]	(6) [OIII] W[ $\text{\AA}$ ]	(7) H $\alpha$ W[ $\text{\AA}$ ]	(8) [SII] W[ $\text{\AA}$ ]	(9) F(H $\beta$ ) <sub>obs</sub> [erg s <sup>-1</sup> cm <sup>-2</sup> ]	(10) r <sub>HII</sub> [ $''$ ]	(11) type
HS1442+4250	-14.73	0.0025	0.081	113	550	574	17	2.95e-14		SS
HS1444+3114	-19.02	0.0297	0.413	26	60	174	38	2.78e-14	1.7	DANS
HS1502+4152	-16.66	0.0164	0.515	7	39	55	21	2.22e-15		DHIIIH
HS1507+3743	-17.58	0.0322	0.114	232	1374	1307	68	3.45e-14	1.0	DHIIIH
HS1529+4512	-17.05	0.0231	0.222	16	99	102	12	2.95e-15	1.7	HIH/DHIIIH
HS1544+4736	-17.11	0.0195	0.025	32	154	162	30	1.00e-14	2.6	DHIIIH
HS1546+4755	-17.78	0.0377	0.485	35	181	204	27	7.77e-15	0.7	DHIIIH
HS1609+4827	-17.6	0.0096	0.381	12	40	86	20	1.91e-14	2.5	HIH
HS1610+4539	-17.2	0.0196	0.480	26	106	152	24	1.41e-14	1.3	DHIIIH/HIIIH
HS1614+4709	-13.6	0.0026	0.100	140	880	915	55	6.62e-14	1.6	SS
HS1633+4703	-15.93	0.0086	0.364	15	55	83	19	1.34e-14	1.1	DHIIIH
HS1640+5136	-19.59	0.0308	0.443	21	55	167	34	2.42e-14	2.0	SBN/HIIIH
HS1641+5053	-19.05	0.0292	0.574	15	65	110	21	2.11e-14		HIH
HS1645+5155	-19.11	0.0286	0.330	47	191	265	45	1.53e-14	5.5	HIH
HS1657+5735	-20.60	0.0505	0.455	43	167	253	46	5.43e-14	1.2	SBN
HS1723+5631A	-18.70	0.0286	0.341	23	100	121	20	1.13e-14		IP
HS1723+5631B	-18.70	0.0286	0.337	32	140	188	32	1.16e-14		IP
HS1728+5655	-16.38	0.0160	0.094	106	514	522	36	2.39e-14	0.9	DHIIIH

Table 4

(1) Galaxy	(2) [OII] 3727	(3) [NeIII] 3869	(4) H $\delta$ 4102	(5) H $\gamma$ 4340	(6) [OIII] 4363	(7) [OIII] 4959	(8) [OIII] 5007	(9) HeI 5876	(10) [OI] 6300	(11) [OI] 6364	(12) [NII] 6584	(13) HeI 6678	(14) [SII] 6717 6731	(15) HeI 7065	(16) [AIII] 7136	(17) [OII] 7320 7330	(18) [AIII] 7751
HS1222+3741	168	68	22	45	15	185	556	10	4	-	-	-	16	-	5	-	-
HS1223+3938	379	75	-	36	-	177	509	17	-	-	-	-	38	-	3	-	-
HS1232+3846	334	-	-	32	-	38	103	-	-	-	68	-	109	-	-	-	-
HS1232+3947	256	-	-	34	-	140	427	14	16	-	5	9	21	-	-	-	-
HS1232+3612	428	69	-	43	-	132	399	9	13	-	27	7	56	-	4	-	-
HS1236+3821	849	-	-	-	-	127	380	11	8	-	19	-	73	-	-	-	-
HS1236+3937	116	78	27	51	14	152	445	13	-	-	-	-	26	-	-	-	-
HS1240+3755	659	-	-	-	-	76	94	-	-	-	179	-	96	-	-	-	-
HS1244+3648	292	55	-	41	-	135	406	15	16	7	-	-	72	-	5	-	-
HS1256+3505	467	-	-	60	-	87	251	15	7	-	63	-	73	-	9	-	-
HS1258+3438	222	43	23	48	2	193	534	10	-	-	-	-	22	-	-	-	-
HS1301+3312	439	-	-	44	-	131	393	9	17	-	-	-	58	-	-	-	-
HS1301+3325	508	-	-	-	-	125	350	-	-	-	-	-	28	-	-	-	-
HS1301+3209	912	-	-	-	-	99	287	-	19	-	10	-	52	-	-	-	-
HS1304+3529	185	55	24	46	10	152	451	10	9	-	10	1	33	-	6	-	-
HS1306+3320	354	53	-	50	-	108	320	11	7	-	-	-	37	-	8	-	-
HS1308+3044	577	-	-	-	-	70	198	-	-	-	59	-	68	-	-	-	-
HS1311+3628	216	29	30	54	-	176	492	11	4	-	13	3	28	-	9	3	-
HS1312+3847	242	64	18	46	5	153	445	18	6	-	10	-	47	-	7	-	-
HS1312+3508	261	64	29	53	7	170	492	12	5	3	11	5	30	4	11	5	4
HS1315+3132	410	20	24	50	5	123	356	11	10	-	-	-	42	-	8	-	-
HS1318+3239	156	63	27	44	12	198	577	13	-	-	-	3	23	-	6	-	-
HS1319+3224	124	63	26	48	13	163	503	10	-	-	-	-	14	-	-	-	-
HS1325+3225	353	-	-	44	-	84	250	10	-	-	-	3	40	-	-	-	-
HS1325+3255	126	57	22	49	8	187	548	9	6	-	-	-	12	-	-	-	-
HS1327+3126	199	56	26	46	7	182	536	12	5	4	-	3	25	3	5	3	2
HS1328+3424	434	-	-	-	-	84	183	-	-	-	34	-	25	-	-	-	-
HS1329+3703	366	-	-	-	-	35	102	-	-	-	85	-	111	-	-	-	-
HS1330+3651	186	48	25	43	9	164	490	15	8	-	9	-	35	-	4	-	-
HS1332+3426	359	74	-	53	-	162	455	14	11	-	-	-	23	-	6	2	-
HS1334+3957	288	48	33	55	-	178	519	17	-	-	5	-	24	-	7	-	-

A spectrophotometric catalogue of HII galaxies

Table 4 (continued)

(1)	(2)	(3)	(4)	(5)	(6)	(7)	(8)	(9)	(10)	(11)	(12)	(13)	(14)	(15)	(16)	(17)	(18)
Galaxy	[OII]	[NeIII]	H $\delta$	H $\gamma$	[OIII]	[OIII]	[OIII]	HeI	[OI]	[OI]	[NII]	HeI	[SII]	HeI	[AIII]	[OII]	[AIII]
	3727	3869	4102	4340	4363	4959	5007	5876	6300	6364	6584	6678	6724	7065	7136	7320	7751
													6731			7330	
HS1336+3114	278	-	-	-	-	79	172	-	-	-	51	-	163	-	-	-	-
HS1340+3307	503	153	-	66	-	174	485	16	-	-	7	-	49	-	-	-	-
HS1341+3409	573	88	-	-	-	126	325	18	-	-	-	-	60	-	-	-	-
HS1347+3811	229	90	28	54	7	189	546	13	8	-	-	-	33	3	8	-	-
HS1349+3942	556	-	-	53	-	106	286	13	12	-	26	-	82	-	-	-	-
HS1354+3634	467	-	-	48	-	91	255	10	18	-	44	-	71	-	-	-	-
HS1354+3635	468	-	-	48	-	118	339	10	7	-	28	3	61	-	4	-	-
HS1402+3650	483	85	-	49	-	96	294	12	13	-	20	4	63	-	-	-	-
HS1410+3627	601	-	-	46	-	109	305	14	14	-	14	-	81	-	-	-	-
HS1413+4402	214	-	-	-	-	26	45	-	-	-	150	-	62	-	-	-	-
HS1416+3554	593	87	-	-	-	99	284	-	-	-	18	-	77	-	-	-	-
HS1420+3437	484	-	-	49	-	79	196	11	-	-	22	-	34	-	-	-	-
HS1422+3325	479	-	-	50	-	90	245	9	-	-	59	-	86	-	-	-	-
HS1422+3339	466	-	-	40	-	105	289	-	-	-	21	-	65	-	-	-	-
HS1424+3836	115	36	26	53	7	181	552	12	4	-	-	-	12	-	3	-	-
HS1425+3835	586	-	-	-	-	59	200	-	-	-	40	-	51	-	-	-	-
HS1429+4511	205	-	-	-	-	11	51	-	-	-	82	-	112	-	-	-	0
HS1429+3154	392	-	-	46	-	142	419	6	6	-	19	-	49	-	7	-	-
HS1438+3147	335	71	-	43	-	174	507	14	8	-	7	-	42	-	-	-	-
HS1440+4302	530	94	26	60	14	191	558	10	6	-	11	-	36	-	7	-	-
HS1440+3120	156	59	30	44	11	211	613	13	5	-	-	3	20	-	4	-	-
HS1440+3805	397	-	-	-	-	78	159	13	23	-	50	-	118	-	-	-	-
HS1442+4250	97	50	22	38	11	165	475	12	-	-	-	2	8	-	4	-	-
HS1444+3114	492	30	-	50	-	75	220	9	9	5	43	-	71	-	6	-	-
HS1502+4152	-	-	-	-	-	153	420	-	-	-	22	-	108	-	-	-	-
HS1507+3743	87	66	29	52	12	217	658	10	3	-	-	2	13	4	4	4	-
HS1529+4512	465	76	-	46	-	173	502	-	-	-	16	-	34	-	-	-	0
HS1544+4736	104	-	-	62	-	147	456	15	7	-	14	-	52	-	7	-	-
HS1546+4755	397	73	40	52	-	166	494	10	7	-	6	-	37	-	-	-	-

Table 4 (continued)

(1)	(2)	(3)	(4)	(5)	(6)	(7)	(8)	(9)	(10)	(11)	(12)	(13)	(14)	(15)	(16)	(17)	(18)
Galaxy	[OII] 3727	[NeIII] 3869	H $\delta$ 4102	H $\gamma$ 4340	[OIII] 4363	[OIII] 4959	[OIII] 5007	HeI 5876	[OI] 6300	[OI] 6364	[NII] 6584	HeI 6678	[SII] 6724 6731	HeI 7065	[AIII] 7136	[OII] 7320	[AIII] 7751 7330
HS1609+4827	551	-	-	38	-	91	261	8	15	-	-	-	63	-	-	-	-
HS1610+4539	390	-	31	47	9	136	374	10	10	-	-	4	42	-	4	-	-
HS1614+4709	79	54	27	50	6	200	590	10	4	-	-	-	18	-	5	-	-
HS1633+4703	596	86	-	48	-	116	309	15	10	-	19	9	67	-	7	-	-
HS1640+5136	520	22	-	56	-	84	243	15	11	4	98	-	79	-	5	-	-
HS1641+5053	582	94	-	33	-	121	339	11	11	-	-	-	50	-	-	-	-
HS1645+5155	349	-	24	45	9	129	387	22	7	-	12	-	46	-	-	-	-
HS1657+5735	349	39	22	47	3	117	355	10	7	1	-	2	47	-	3	-	2
HS1723+5631A	425	-	-	61	-	140	412	15	14	6	23	-	49	-	-	-	-
HS1723+5631B	352	-	-	54	-	144	419	13	9	-	23	-	50	-	-	-	-
HS1728+5655	211	75	26	47	3	172	500	12	5	2	25	2	23	-	7	3	-

Table 5

(1) Galaxy	(2) $M_B$	(3) $z$	(4) $H\beta$ W [Å]	(5) [OIII] W [Å]	(6) $H\alpha$ W [Å]	(7) [SII] W [Å]	(8) $F(H\beta)_{obs}$ [erg s <sup>-1</sup> cm <sup>-2</sup> ]	(9) [OII] 3727	(10) $H\gamma$ 4340	(11) [OIII] 4959	(12) [OIII] 5007	(13) HeI 5876	(14) [OI] 6300	(15) $H\alpha^*$ 6563 6584	(16) HeI 6678	(17) [SII] 6724 6731	(18) $r_{HII}$ ["]	(19) type
HS1255+3506	-16.61	0.0155	10	31	66	19	4.70e-15	381	-	86	258	-	24	457	-	124	1.7	DHIII?
HS1318+3406	-18.65	0.0352	8	17	69	21	5.09e-15	414	-	74	178	-	-	526	-	152		IIII?
HS1327+3412	-	0.2510	11	7	111	11	-	87	-	13	52	-	-	376	-	37	0.7	-
HS1333+3149	-18.61	0.0248	8	27	66	11	8.86e-15	387	-	101	267	-	-	470	-	77	2.3	IIII
HS1340+3207	-18.35	0.0365	18	105	127	23	6.92e-15	390	16	186	555	21	-	426	-	73	1.7	DANS
HS1429+3154*	-16.73	0.0117	34	144	162	26	2.06e-14	347	39	143	424	6	7	344	-	55	2.6	DHIII
HS1442+4332	-20.05	0.0811	5	9	65	15	2.55e-15	361	-	57	116	15	43	616	14	126	1.5	SBN?
HS1543+4525	-19.17	0.0389	10	15	92	27	6.90e-15	388	-	38	123	15	14	573	8	164	2.2	DANS?
HS1627+5239*	-17.88	0.0288	14	37	95	16	7.61e-15	286	-	73	224	12	-	422	-	70	1.22	IIII?
HS1657+5033	-17.43	0.0102	7	29	60	14	1.19e-14	338	-	103	323	10	-	559	6	124	1.88	IIII

The galaxies HS1429+3154 and HS1627+5239 have detected [AIII]  $\lambda$ 7136, with the line ratios relative to  $H\beta$  of 8 and 15, respectively.

Table 6

(1) Galaxy	(2) $M_B$	(3) $z$	(4) $F(H\alpha)_{obs}$ [erg s <sup>-1</sup> cm <sup>-2</sup> ]	(5) [OII] 3727	(6) [OIII] 5007	(7) [NII] 6584	(8) [SII] 6724 6731	(9) $r_{HII}$ ["]	(10) type
HS1309+3409	-20.19	0.0785	1.59e-14	-	-	41	14	1.5	SBN
HS1331+3906	-20.37	0.0643	1.11e-14	-	-	37	33	2.4	SBN
HS1336+3650	-16.84	0.0202	3.16e-15	-	114	-	-	1.5	DHIII
HS1421+4018	-	0.0982	6.12e-15	132	-	-	84		
HS1435+4523	-20.29	0.1267	8.69e-15	60	22	26	65	1.9	SBN
HS1505+3944	-18.47	0.0366	5.20e-15	40	-	-	-	2.8	DANS/IP
HS1522+4214	-17.76	0.0190	3.74e-15	79	31	29	55	1.85	DANS/DHIII



### 3. The catalogue

The Catalogue is presented in Table 3 through Table 6. Table 3 and 4 present the spectroscopic parameters of all the galaxies for which a reliable internal extinction correction was done, and which account for the main body of the Catalogue. The data are arranged in Table 3 as follows:

- Col. 1: The galaxy name according to Popescu et al. (1996,1998).
- Col. 2: The absolute blue magnitudes ( $M_B$ ) as listed in Vennik et al. (1999).
- Col. 3: The heliocentric redshift.
- Col. 4: The absorption coefficient  $c(H\beta)$ .
- Col. 5, 6, 7, 8: The equivalent widths (W) of the  $H\beta$ , [OIII]  $\lambda 5007$ ,  $H\alpha$  and [SII]  $\lambda\lambda 6717, 6731$  emission lines in  $\text{\AA}$ .
- Col. 9: The observed  $H\beta$  fluxes in  $\text{erg sec}^{-1}\text{cm}^{-2}$ , corrected for absorption.
- Col. 10: Seeing corrected approximate angular size of the star-forming regions  $r_{HII}$ , as measured in the B band by Vennik et al. (2000).
- Col 11: The morphological type.

Table 4 contains the corrected line ratios (normalised to  $H\beta = 100$ ) of the emission lines detected in the spectra of the galaxies listed in Table 3. The header of the table contains the identification of the emission line while the line below gives the corresponding restframe wavelength. The [SII]  $\lambda\lambda 6724, 6731$  and the [OII]  $\lambda\lambda 7320, 7330$  are not deblended, and therefore the line ratios refer to their blend.

Table 5 lists the galaxies for which it was not possible to deblend  $H\alpha$  from [NII]  $\lambda\lambda 6563, 6584$ , and therefore the line ratios were not corrected for internal extinction. The line ratio of  $H\alpha$  corresponds to the blend with the [NII] lines. Finally, Table 6 lists those galaxies for which the  $H\beta$  emission line was too noisy to allow an accurate determination of the internal extinction, and again only the uncorrected line ratios are listed. Here, the line ratios in column 5 through 8 are given in units of  $H\alpha = 100$ .

In 8 cases it was possible to disentangle the contribution of different HII regions in the galaxy. Then the spectrum of each region was extracted separately and the fluxes measured for each individual region. In Tables 3-6 only the line ratios corresponding to the brightest HII region are given, but the  $H\beta$  fluxes are the total fluxes for the galaxy, summed over all the HII regions. In Table 7 we list the 8 galaxies with detected HII regions together with their observed  $H\beta$  fluxes. These fluxes are not corrected for absorption. The HII regions are given in order of their location along the slit, from South to North.

### 4. Wolf-Rayet galaxies

Some of our galaxies show the broad HeII  $\lambda 4686$  feature, which is a direct signature from Wolf-Rayet (WR) stars. For low resolution spectroscopy (as in the case of our spectra) this line is usually seen as a WR bump, a blend of HeII

**Table 7**

Galaxy	$F(H\beta)_{obs}$ [ $\text{erg sec}^{-1}\text{cm}^{-2}$ ]			
	HII1	HII2	HII3	HII4
HS1232+3846	4.25e-16	2.33e-15	4.19e-16	3.62e-16
HS1236+3821	5.01e-15	1.90e-16		
HS1244+3648	1.25e-15	1.39e-14		
HS1304+3529	2.57e-15	4.42e-14	1.45e-15	
HS1312+3508	2.12e-15	1.00e-13		
HS1340+3307	6.20e-16	9.11e-15		
HS1614+4709	5.92e-14	1.17e-15	5.81e-15	
HS1641+5053	1.37e-15	1.73e-14		

and other broad stellar emission lines from CIII, NIII and NV, but also of narrow nebular emission lines including HeII  $\lambda 4686$ . The galaxies with detected WR features are listed in Table 8 with the flag D (detection), while a few more candidates for WR galaxies are also listed in Table 8, with the flag C (candidates). For some of the galaxies with detected WR features we also list the line ratios (corrected for internal extinction) relative to  $H\beta=100$ . The first galaxy from the table, HS0915+5540, does not belong to the spectrophotometric catalogue presented in this paper, but to the larger catalogue of emission-line galaxies from which the present catalogue was selected (Popescu et al. 1996).

**Table 8**

Galaxy	Intensity <sup>a</sup>
HS0915+5540	D
HS1304+3529	D 5
HS1312+3847	C
HS1312+3508	D 4
HS1424+3836	D 9
HS1442+4250	C
HS1507+3743	D 6
HS1657+5735	D 4
HS1728+5655	C

<sup>a</sup> Dereddened line fluxes relative to  $I(H\beta)=100$ .

In total we detected 6 new WR galaxies and 3 candidates for WR galaxies. This represent 5.5% from our spectrophotometrical catalogue, or 9%, if we include the candidates, too. Such a detection rate is somewhat lower than the detection rate of 10% obtained by Masegosa et al. (1991) for a systematic search for broad WR bump in the HII galaxies. However our spectral resolution is very low and it is therefore not optimised for this kind of search, and these results came only serendipitously.

The total number of known WR galaxies and extragalactic HII regions showing broad HeII  $\lambda 4686$  emission is 139 (from the recent compilation of Schaerer et al. (1999)). These objects are found among a large variety of morphological types, from BCDs and Im galaxies to massive spirals and luminous IRAS galaxies, and even in Seyfert 2 and LINERSs (Osterbrock & Cohen 1982, Kunth & Contini 1998). Extending the sample of WR galaxies is very useful in constraining the evolution of massive stars and the parameters of the upper part of the IMF. Also, as discussed by Schaerer et al. (1999), WR galaxies represent useful templates of young starburst galaxies, which may be used to explain the properties of the distant star-forming galaxies.

Among the galaxies with detected WR features we found one SBN galaxy (HS1657+5735), a DANS galaxy (HS0915+5540), three DIIH galaxies (HS1312+3508, HS1424+3836, HS1507+3743), and an interacting pair, IP (HS1304+3529). The candidates for WR features are SS, HIIH and DIIH galaxies. Thus it is probably reasonable to conclude that WR phenomenon is spread over all morphological subtypes of BCDs.

## 5. Candidates for very low metallicities

There has been a long debate on whether the BCDs are truly young dwarf galaxies undergoing their first burst of star formation or whether the present burst occurs within an older galaxy. The low abundances found in these galaxies make them good candidates for the least chemically evolved galaxies. But the detection of an extended faint stellar underlying component in the majority of BCDs (Loose & Thuan 1986, Kunth et al. 1988, Telles et al. 1997, Vennik et al. 1999) supports the idea that they are not truly primordial galaxies, but older LSB dwarf galaxies undergoing transient periods of star formation. A clear demonstration of this two - component structure was recently presented by Schulte-Ladbeck et al. (1998, 1999) for the very nearby BCD VII Zw 403 (UGC 6456), based on HST photometry of its individual stars down to the red giant branch stars. Even for I Zw 18, the lowest metallicity known galaxy, Garnett et al. (1997) found C/O to be much larger than the mean value of other metal-deficient galaxies. This was interpreted as a proof that I Zw 18 has experienced carbon-enriching episodes of star formation in the past, and is therefore not a young galaxy. Recently Aloisi et al. (1999) used synthetic colour-magnitude diagrams to investigate deep HST data for I Zw 18, and they found again that the present burst is not the first one to occur in this galaxy.

However, Izotov & Thuan (1999) argued that the extreme low metallicity BCD SBS 0335-052 is a good example for a young galaxy; the HST V and I imaging of this galaxy (Thuan et al. 1997) showed extremely blue colours, not only in the region of current star formation but also in the extended low surface brightness underlying

component. Thuan & Izotov (1997) also argued that the large HI cloud associated with this BCG (Pustilnik et al. 1999) is made of pristine gas, unpolluted by metals. Based on abundance measurements, Izotov & Thuan (1999) suggested that in fact all galaxies with  $12+\log(\text{O}/\text{H}) \leq 7.6$  are young, with ages not exceeding 40 Myr, while those with  $7.6 < 12 + \log(\text{O}/\text{H}) < 8.2$  are not older than 1-2 Gyr. Furthermore, Lynds et al. (1998) discussed the possibility that VII Zw 403 (UGC 6456) is not young (as also found by Schulte-Ladbeck et al. 1998, 1999), but could still be considerably younger than a Hubble time.

While the controversy on the age of the BCDs reflects our current knowledge of galaxy formation and evolution (Schulte-Ladbeck et al. 1999), more work on both statistical samples of very low-metallicity BCDs as well as HST imaging of nearby BCDs could give clues relevant to this debate. In this section we give a list of candidates for very-low metallicity BCDs, which were found in the spectroscopical analyses of our sample. Nevertheless, high-resolution spectroscopy is needed to confirm the metallicity that we assign for each object.

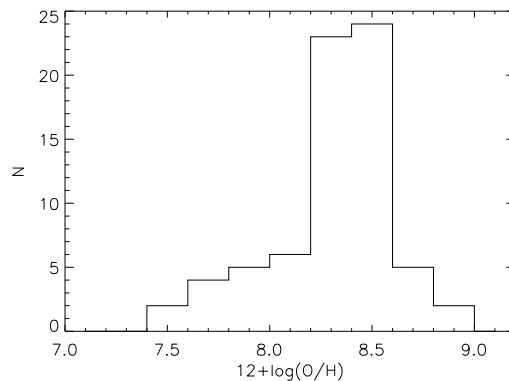


**Fig. 1.** The distribution of the oxygen abundances  $12+\log(\text{O}/\text{H})$ .

We derived the metallicities for our sample using both the models of Dopita & Evans (1986) as well as a five level atom program and the ionisation correction method of Mathis & Rosa (1991), the latter for the few objects for which the [OIII]  $\lambda 4363$  line was detected in the spectrum. The distribution of  $12+\log(\text{O}/\text{H})$  (Fig. 1) has a maximum around 8.5, with a long tail towards low and very low metallicities. All the galaxies with metallicities less than 8.0 were considered candidates for very low metallicity objects and are listed in Table 9. The value of the metallicity we assign should be taken with caution, and only as a preliminary result. As a simple consistency check, we used the data from Table 9 to plot the metallicity - luminosity relation of star forming dwarf galaxies, as given by Skillman et al. (1989). Since the dwarf galaxies used by Skillman et al. are all dwarf irregular galaxies, we further added some BCD's from Thuan et al. (1997). Our data distribute in the same region as the Thuan et al.

BCDs, with a similar amount of scatter and are - within the errors - in good agreement to the relation proposed by Skillman et al. (1989) (see Fig. 2). We conclude that the errors in our preliminary  $12+\log(\text{O}/\text{H})$  determinations are small enough to indicate the existence in our sample of some interesting low-abundance BCDs. However, we can not exclude a small offset in our O/H scale.

**Table 9.** Candidates for very low metallicity galaxies

Galaxy	$12+\log(\text{O}/\text{H})$	$M_B$
HS1222+3741	7.64	-17.67
HS1236+3937	7.47	-15.67
HS1304+3529	7.66	-17.38
HS1318+3239	7.81	-17.22
HS1319+3224	7.59	-15.3
HS1330+3651	7.66	-17.15
HS1347+3811	7.94	-15.30
HS1424+3836	7.97	-16.06
HS1440+3120	7.91	-17.4
HS1442+4250	7.89	-14.73
HS1507+3743	7.74	-17.58

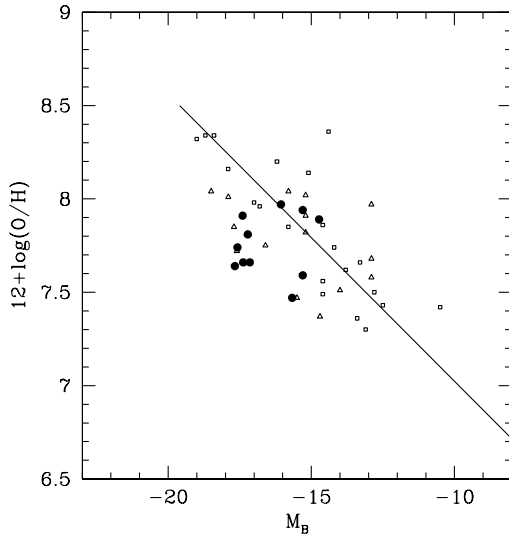


**Fig. 2.** The oxygen abundances ( $12+\log(\text{O}/\text{H})$ ) - absolute magnitude relation as derived by Skillman et al. (1989) for the local dwarf irregular galaxies (open squares). Some selected BCDs from Thuan et al. (1997) are also plotted (open triangles) together with our low-abundance candidates (filled dots).

## 6. The properties of the sample

In this section we present some statistics on the relevant spectroscopic parameters of the sample as well as of subsamples of different morphological subtypes.

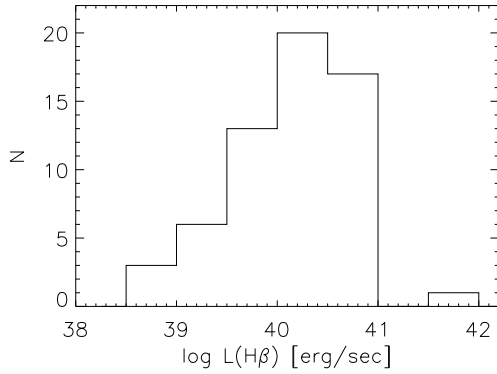
Our sample was selected in certain fields which contain huge underdensities. One concern is that its galaxy content is thus different from the galaxy content of samples selected from the general field environment. In passing we should note that Popescu et al. (1997) found that most of our sample galaxies belong to the normal field features of the large scale structure. Nevertheless, we make an extra check, by comparing the frequency distribution of the Salzer et al. (1989b) types (see Tables 3, 5, and 6) with those from the University of Michigan (UM) survey, which is a general field survey. The comparison is given in Table 10 and indicates little significant differences in the type distribution of the two samples. If at all, we have some more DHIIH galaxies and fewer SBN objects in our sample. This is to be expected due to the selection criteria we adopted, namely bright objects were excluded from the survey (Popescu et al. 1996). The motivation was that bright objects were already included in other catalogues and we were mainly interested in dwarf galaxies. Since the frequency distribution of different morphological types is very close to that of the UM survey, we also expect a correlation between the Salzer et al. (1989) morphological types of our objects and their absolute blue magnitude. We verified that this correlation exists, but with a reasonable scatter in each sub-class. This scatter (peak-to-peak) can be as large as 4 mag in most of the type bins. For a

**Table 10.** Frequency distribution of the ELG types in the University of Michigan survey (UM) and in our sample.

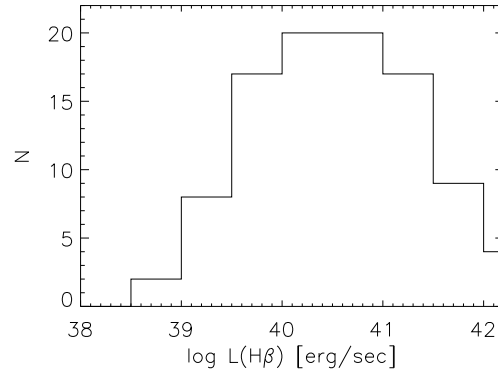
Type	this paper [%]	UM [%]
SS	$4.8 \pm 2.4$	9.9
DHIIH	$39.3 \pm 6.8$	29.7
HIIH	$26.2 \pm 5.6$	24.8
DANS	$14.3 \pm 4.1$	12.4
SBN	$8.3 \pm 3.1$	13.2
IP	$7.1 \pm 2.9$	9.9

detailed discussion of the sample properties as a function of the galaxy density see Popescu et al. (1999).

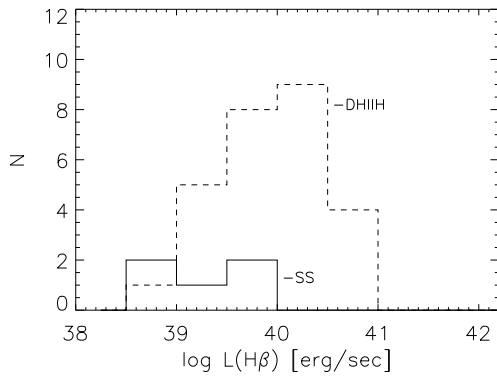
The histogram of the  $H\beta$  luminosities of the whole sample is given in Fig. 3a. The luminosities were calculated for a Hubble constant  $H_0 = 75 \text{ km/s/Mpc}$  and they were corrected for internal extinction. The distribution is asymmetric, with a sharp cut-off towards the brighter end. This is due to the selection criteria we adopted, as mentioned above (see also Popescu et al. 1996). The in-



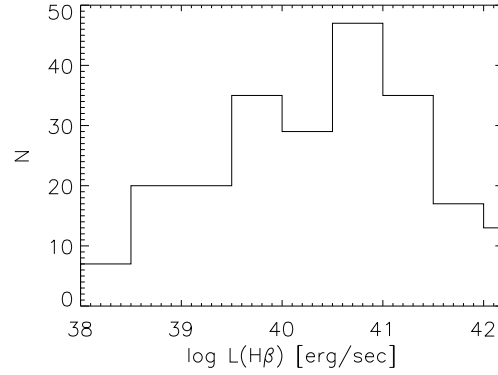
(a) The distribution of the  $H\beta$  luminosities. The luminosities have been corrected for internal absorption.



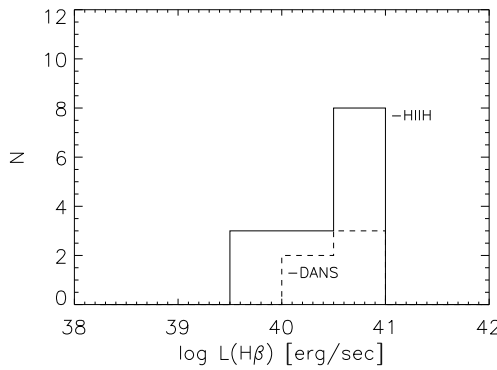
(d) The distribution of the  $H\beta$  luminosities for the sample of Salzer et al. (1989).



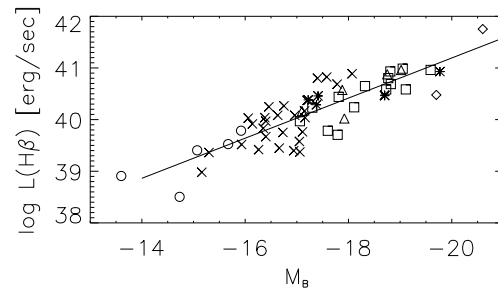
(b) The distribution of the  $H\beta$  luminosities for SS and DIIIH galaxies. The luminosities have been corrected for internal absorption



(e) The distribution of the  $H\beta$  luminosities for the sample of Terlevich et al. (1991).



(c) The distribution of the  $H\beta$  luminosities for HIII and DANS galaxies. The luminosities have been corrected for internal absorption



(f) The logarithm of the  $H\beta$  luminosities as a function of blue absolute magnitude. The different symbols indicate the ELG type:  $\circ$  - Searle-Sargent Galaxy,  $\times$  - Dwarf HII Hotspot Galaxy,  $\square$  - HII Hotspot Galaxy,  $\triangle$  - Dwarf Amor. Nuclear Starburst,  $\diamond$  - Starburst Nucleus,  $*$  - Interacting Pair. The solid line represent a linear least-square fit to the data.

completeness at the bright end is also obvious when compared with the  $H\beta$  distribution of other similar samples from the literature. For example, in Fig. 3d we show, for comparison, the  $H\beta$  luminosity distribution of a sample of 99 ELGs (Salzer et al. 1989b) from the UM objective-prism survey and in Fig. 3e the same distribution from the ELG sample of Terlevich et al. (1991). In comparison with our distribution, the latter ones are more symmetrical and span over more orders of magnitude. They include at the bright end also Seyfert galaxies, which were not included in our study. The  $H\beta$  luminosity distributions of different morphological subtypes are shown in Fig. 3b (for SS and DHIIH galaxies) and in Fig. 3c (DANS and HIIIH), respectively. The differences between them show the known trend of increasing  $H\beta$  luminosities from the SS to DANS class, though a significant overlap exist, too.

The expected correlation between the  $H\beta$  luminosities and the blue magnitudes is shown in Fig. 3f, where different morphological subtypes are plotted with different symbols. A linear least square fit to the  $\log(L(H\beta))=f(M_B)$  data (plotted with solid line) gives a slope of -0.388 and a correlation coefficient of 0.85. This is close to the the slope (-0.391) of a similar correlation found by Salzer et al. (1989b) for the ELGs of the Michigan Survey. The slope of -0.391 was derived when the Seyfert and SS galaxies were excluded from the correlation. This is consistent with our set of data, which does not contain Seyfert galaxies. Also the SS galaxies of our sample seem to follow in a better way the correlation, while those found by Salzer are lying mainly in the upper part of the correlation. As remarked by Salzer, this slope suggests that, within the uncertainties, the  $H\beta$  luminosity scales directly with the blue luminosity:  $L(H\beta) \propto L_B$ . This would indicate that the recent star-formation (in the last  $\sim 10$  Myr) and the integrated star-formation are related. On the other hand the scatter from the correlation suggests variations in the global equivalent widths,  $W(H\beta)$ , which means different stages of activity. If the total blue magnitude is a good measure of the average past star formation, then the scatter indicates an intrinsic variation in the ratio between the present star formation rate and the average past.

The distribution of the  $H\beta$  equivalent widths is also given in Fig. 4.

## Appendix

During our survey for emission line galaxies we also identified a few quasars and AGNs. Here we give some spectroscopic information about a peculiar QSO found in our survey, namely HS1643+5313. This object looked peculiar also in the objective-prism scans, in the sense that it displayed a double peaked feature, just at the green head of the objective prism spectrum. A first possibility would have been that the strongest feature were the  $[OIII]\lambda 5007$  line of a narrow-emission line galaxy while the second feature a cosmic or only noise. No other combination of

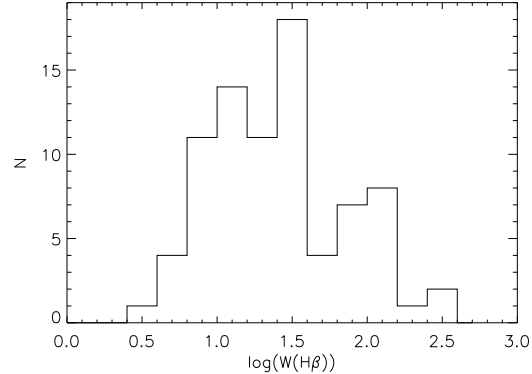


**Fig. 4.** The distribution of the  $H\beta$  equivalent widths (in units of  $\text{\AA}$ ).

emission-lines at any redshift and at this dispersion were known to fit the above mentioned spectrum. The spectrum was therefore chosen mainly with the hope of being still a narrow-emission line galaxy. The slit spectrum (Fig. 5) displays the same combination of a double emission-line feature. After analysing in detail the spectrum as well as its direct image we reached the conclusion that the object is a QSO at  $z=0.785$ , the emission-features being thus only one line, namely the  $MgII \lambda\lambda 2798$  blend, but with an absorption dip inside. There is also some faint detection of  $FeII$  at  $5262 \text{\AA}$ , but the S/N ratio of the spectrum is too poor for a clear detection of further fainter lines. A high resolution spectrum of the near infrared region would clarify whether the absorption is internal to the QSO or arises from a foreground cloud or galaxy.

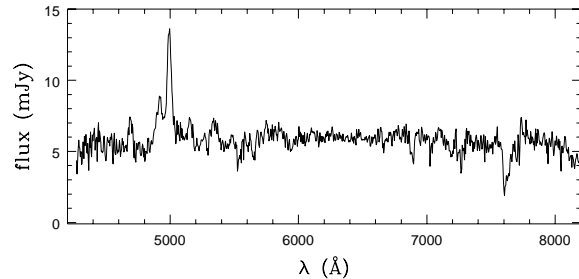


**Fig. 5.** Slit spectrum of the quasar HS1643+5313,  $z=0.785$ .

*Acknowledgements.* U.H. acknowledges the support of the SFB 375.

This research has made use of the NASA/IPAC Extragalactic Database (NED) which is operated by the Jet Propulsion Laboratory, California Institute of Technology, under contract with the National Aeronautics and Space Administration.

## References

- Allen D.A., Wright A.E., Goss W.M., 1976, MNRAS 177, 91
- Aloisi A., Tosi M., Greggio L., 1999, AJ 118, 302
- Binggeli B., Sandage A., Tammann G.A., 1985, AJ 90, 1681

- Brocklehurst M., 1971, MNRAS, 153, 471  
Burstein D., Heiles C., 1984, ApJS 54, 33  
de Lapparent V., Geller M.J., Huchra J.P., 1986, ApJ 302, L1  
Dopita M.A., Evans I.N., 1986, ApJ 307, 431  
Gallagher J.S., Hunter D.A., 1989, AJ 98, 806  
Garnett D.R., Skillman E.D., Dufour R.J., Shields G.A., 1997, ApJ 481, 174  
Hagen H.-J., Groote D., Engels D., Reimers D., 1995, A&AS 111, 195  
Howarth I.D., 1983, MNRAS 1983, 203, 301  
Izotov Y.I., Thuan T., 1999, ApJ 511, 639  
Kunth D., Contini T. 1998, in "Wolf-Rayet Phenomena in Massive Stars and Starburst Galaxies", K.A. van der Hucht, G. Koenigsberger, P.R.J. Eenens (eds), IAU Symp. 193, (San Francisco: ASP), in press  
Kunth D., Maurogordato S., Vigroux L., 1988, A&A 204, 10  
Lequeux J., Peimbert M., Rayo J.F., Serrano A., Torres-Peimbert S., 1979, A&A 80, 155  
Lynds R., Tolstoy E., O'Neil E.J., Hunter D.A., 1998, ApJ 116, 146  
Loose H.-H., Thuan T.X., 1986, ApJ 309, 59  
Masegosa J., Moles M., Del Olmo A., 1991, A&A 244, 273  
Mathis J.S., Rosa M.R., 1991, A&A 245, 625  
McCall M.L., Rybski P.M., Shields G.A., 1985, ApJS, 57, 1  
Oke J.B., 1990, AJ 99, 1621  
Osterbrock D.E., Cohen R.D., 1982, ApJ 261, 64  
Popescu C.C., Hopp U., Elsässer H., 1997, A&A 328, 756  
Popescu C.C., Hopp U., Rosa M., 1999, A&A 350, 414  
Popescu C.C., Hopp U., Hagen H.J., Elsässer H., 1996, A&AS, 116, 43  
Popescu C.C., Hopp U., Hagen H.J., Elsässer, H., 1998, A&AS, 133, 13  
Pustilnik S.A., Thuan T.X., Brinks E., Lipovetsky V.A., Izotov Y.I., 1999, in preparation  
Salzer J.J., MacAlpine G.M., Boroson T.A., 1989a, ApJS 70, 447  
Salzer J.J., MacAlpine G.M., Boroson T.A., 1989b, ApJS 70, 479  
Sargent W.L.W., Searle L., 1970, ApJ, 162, L155  
Schaefer D., Contini T., Pindao M., 1999, A&AS 136, 35  
Schulte-Ladbeck R.E., Crone M.M., Hopp U., 1998, ApJ, 493, L23  
Schulte-Ladbeck R.E., Hopp U., Crone M.M., Greggio L., 1999, ApJ 525, 709  
Skillman E. D., Kennicutt R. C., Hodge P.W., 1989, ApJ 347, 875  
Telles E., Melnik J., Terlevich R., 1997, MNRAS 288, 78  
Terlevich R., Melnick J., Masegosa J., Moles M., Copetti M.V.E., 1991, A&AS 91, 285  
Thuan T.X., Izotov Y.I., Lipovetsky V.A., 1997, ApJ 477, 661  
Vennik J., Hopp U., Popescu C.C., 2000, A&AS submitted  
Vílchez J.M., 1995, AJ 110, 1090  
Whitford A.E., 1958, AJ 63, 201